SUPPORTING INFORMATION

Computational Analysis of the Binding Specificity of Gleevec to Abl, c-Kit, Lck, and c-Src Tyrosine Kinases

Yen-Lin Lin[†] and Benoît Roux[*,†,‡]

[1]Department of Biochemistry and Molecular Biology Gordon Center for Integrative Science, The University of Chicago, 929 57th Street, Chicago, Illinois 60637, USA.

[2]Biosciences Division, Argonne National Laboratory, 9700 South Cass Avenue, Argonne, Illinois 60439, USA

* Corresponding author e-mail: roux@uchicago.edu

[†] the University of Chicago

[‡] Argonne National Laboratory

Contents

Page 3. Time evolution of the root-mean-square deviations (RMSDs) for the heavy atoms of Gleevec and the backbone heavy atoms of Abl, c-Kit, Lck, and c-Src tyrosine kinases from their respective starting structures: Figures S1

Page 4. Superimposing equilibrated and starting conformations of Gleevec in the binding pockets of Abl, c-Kit, Lck, and c-Src: Figures S2

Page 5. Time series of the fluctuations of the six internal coordinates used for the energy restraints of the ligand in the bound complex during the translational and rotational free energy simulations: Figure S3

Page 6. Convergence of the binding affinity of Gleevec with Abl, c-Kit, Lck, and c-Src kinases: Figure S4

Page 7. Progression of the free energy components with respect to the coupling parameters of (A) λ_{rep}, (B) λ_{dis}, (C) λ_{elec}, and (D) λ_{t+r} for Gleevec in the binding sites or in bulk solution: Figure S5

Page 8. Radius of gyration, R_g, for the binding site residues of Abl, c-Kit, Lck, and c-Src as a function of the coupling parameter λ_{rep} during the FEP calculations: Figure S6

Page 9. Snapshot of hydrogen-bonding network in the Gleevec-bound pocket of Abl kinase: Figure S7

Page 10. PMF profiles on the conformational restraints for Gleevec in bulk solution as well as in the binding pockets of the tyrosine kinases: Figure S8

Page 11. RMSD versus simulation time for the backbone heavy atoms of the closed-form (in magenta color) and open-form (in blue color) A-loop in c-Src structure complexed with Gleevec relative to the initial closed c-Src conformation: Figure S9

Page 12. Ribbon diagram of (A) Abl, (B) c-Kit, (C) Lck, and (D) c-Src in complex with Gleevec: Figure S10

Page 13. Reference values of selected internal coordinates for the translational and rotational restraints on the ligand: Table S1

Page 14. Averaged dispersive contributions to the interactions energy between protein residues and Gleevec in the binding pockets of Abl, c-Kit, Lck, and c-Src kinases: Table S2

Page 15. Averaged electrostatic contributions to the interactions energy between protein residues and Gleevec in the binding pockets of Abl, c-Kit, Lck, and c-Src kinases: Table S3

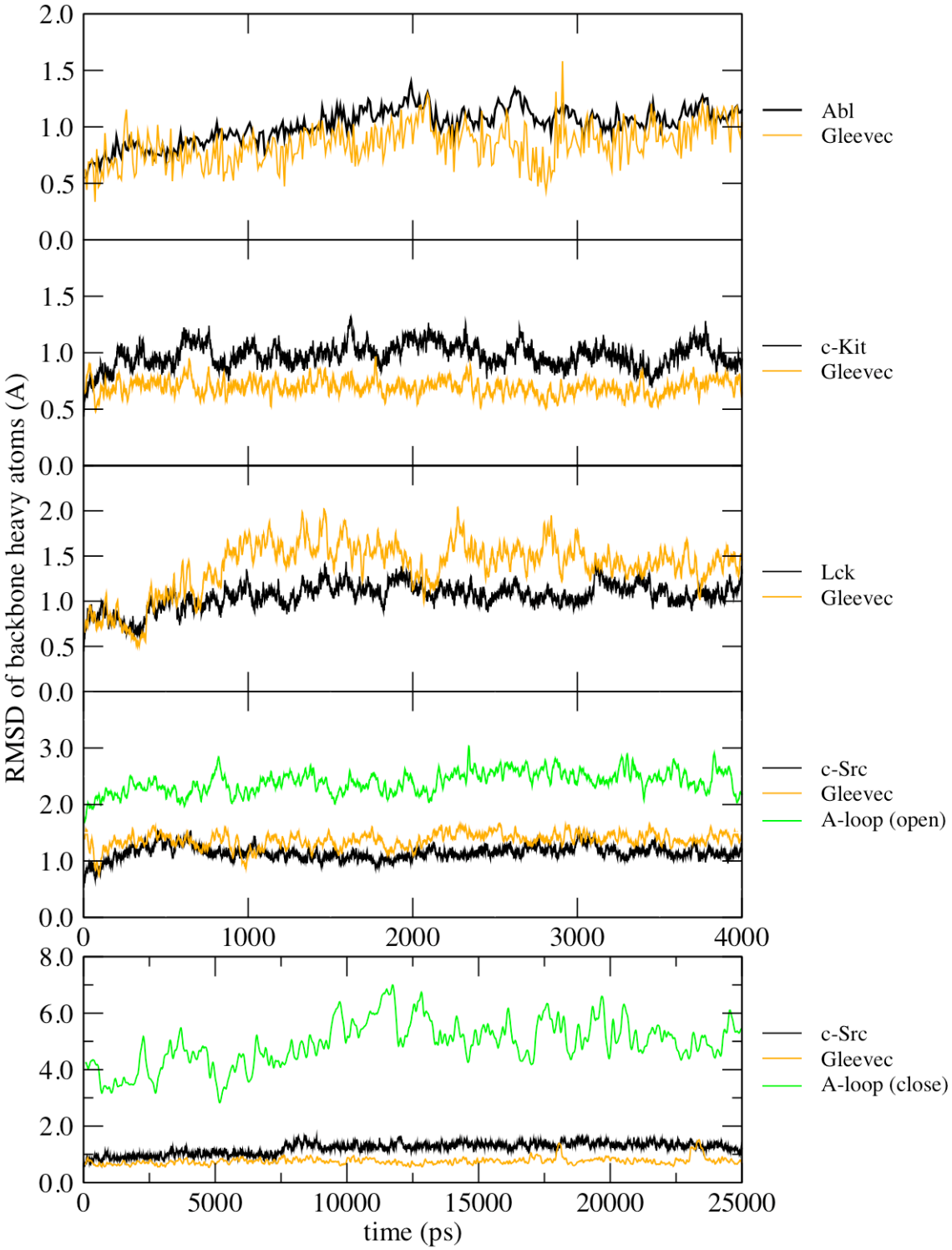

Figure S1: RMSD versus simulation time for the non-hydrogen atoms of Gleevec (orange lines) as well as the backbone heavy atoms of Abl, c-Kit, Lck, and c-Src (black lines) relative to the respective initial X-ray crystal structures. For each system, the RMSD of the non-hydrogen atoms of the protein backbone varies around 1.0 Å during the last 2 ns after the equilibration. The bound ligand generally displays larger RMSD fluctuations at this stage, deviating from 0.4 to 2.2 Å, although the equilibrated conformation in the binding site is well maintained relative to

the experimental starting structure for all systems (see Figure S2 below). The RMSD fluctuations of the activation loop (A-loop) in c-Src(*o*) and c-Src(*c*), represented by green lines, reach to a steady plateau during the equilibration simulations. The overall structures and the position of the bound ligand are stable in the course of the MD trajectories of the protein-ligand complex systems. The well-equilibrated solvated structures are adopted for the following FEP/MD calculations.

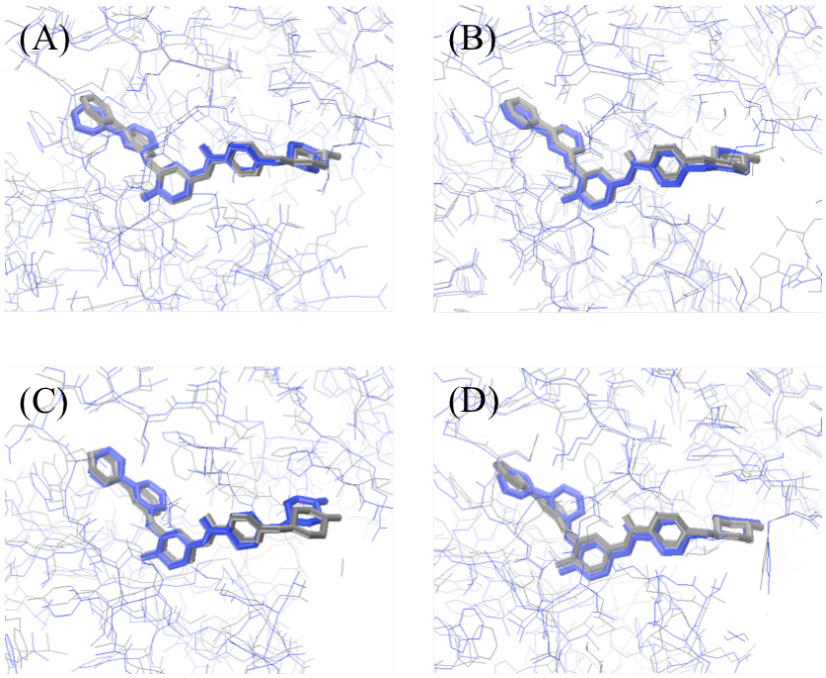

Figure S2: Superimposing equilibrated (blue) and starting (gray) conformations of Gleevec in the binding sites of (A) Abl, (B) c-Kit, (C) Lck, and (D) c-Src. The non-hydrogen atoms of the kinases are represents by lines. Gleevec is represented by thick sticks.

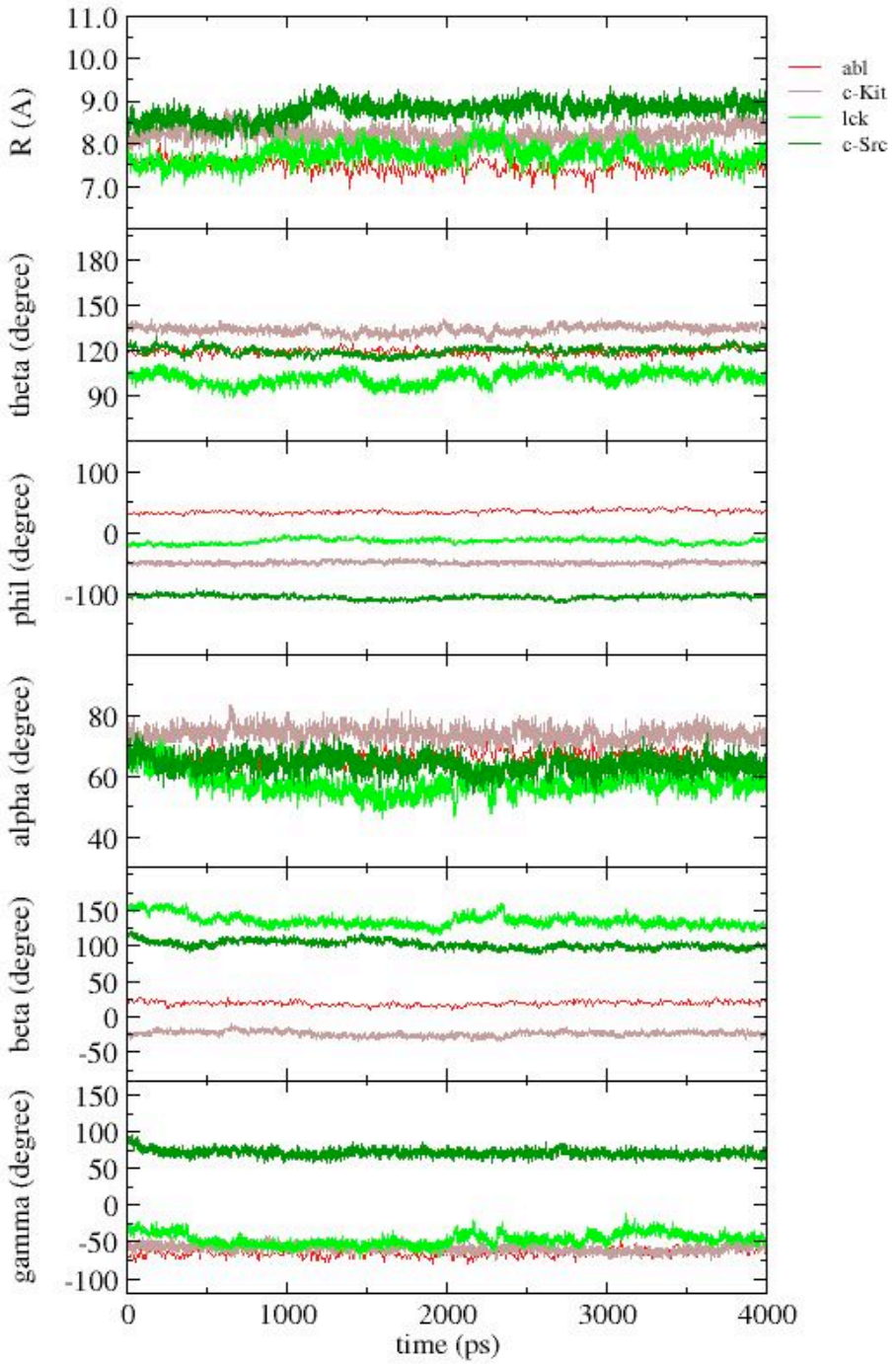

Figure S3: Time series of the fluctuations of the six internal coordinates used for the energy restraints of the ligand in the bound complex during the translational and rotational free energy simulations

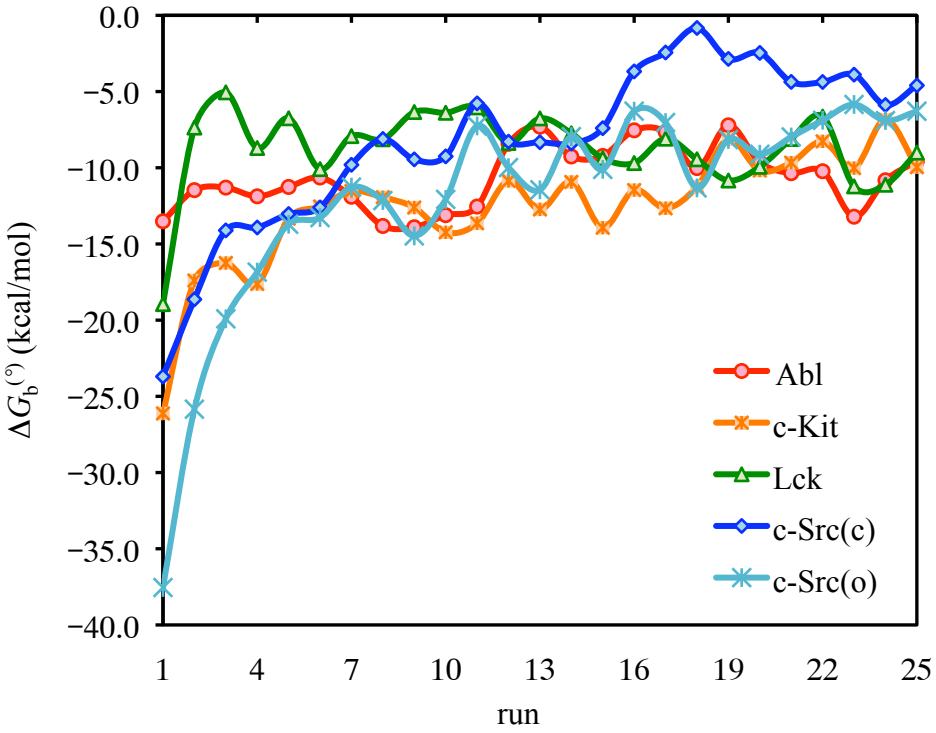

Figure S4: Convergence of the absolute binding free energy calculations of Gleevec, ΔG_b°, with Abl, c-Kit, Lck, c-Src(*c*), and c-Src(*o*)

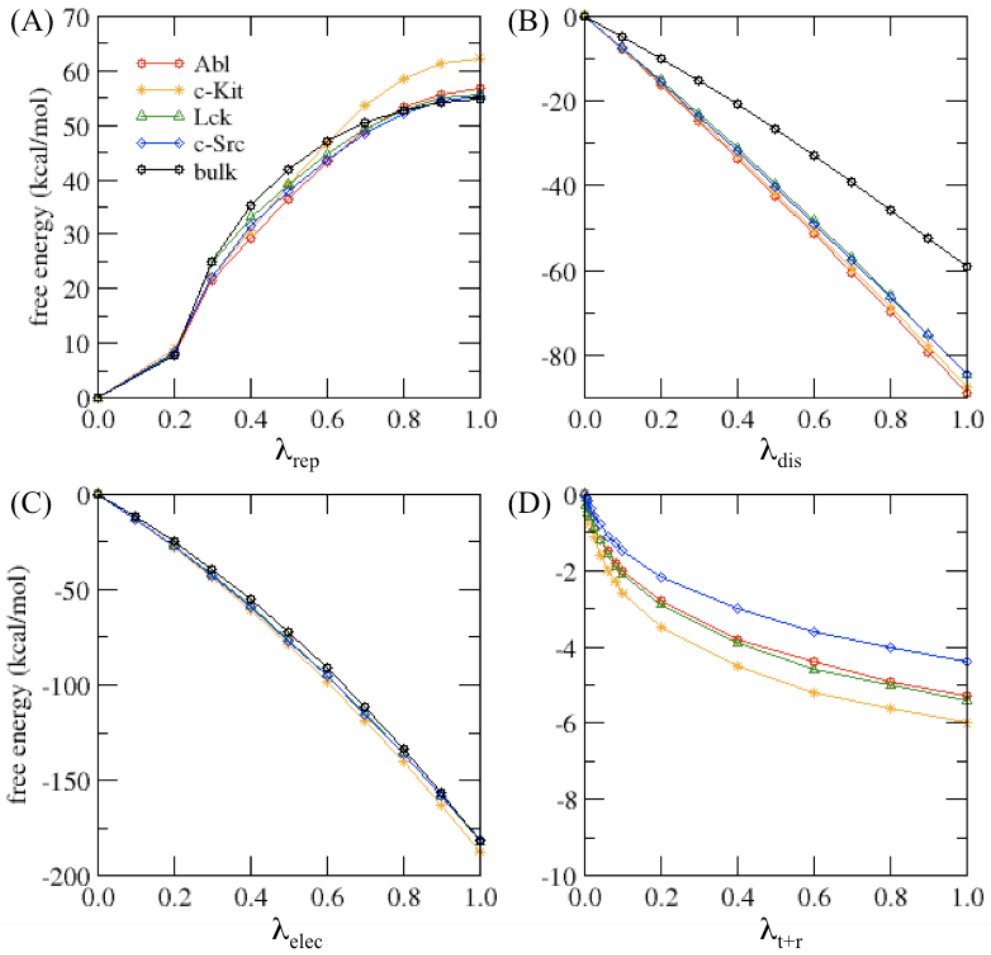

Figure S5: Progression of the free energy components with respect to the coupling parameters of (A) λ_{rep}, (B) λ_{dis}, (C) λ_{elec}, and (D) λ_{t+r} for Gleevec in the binding sites (colored lines) or in bulk solution (black lines)

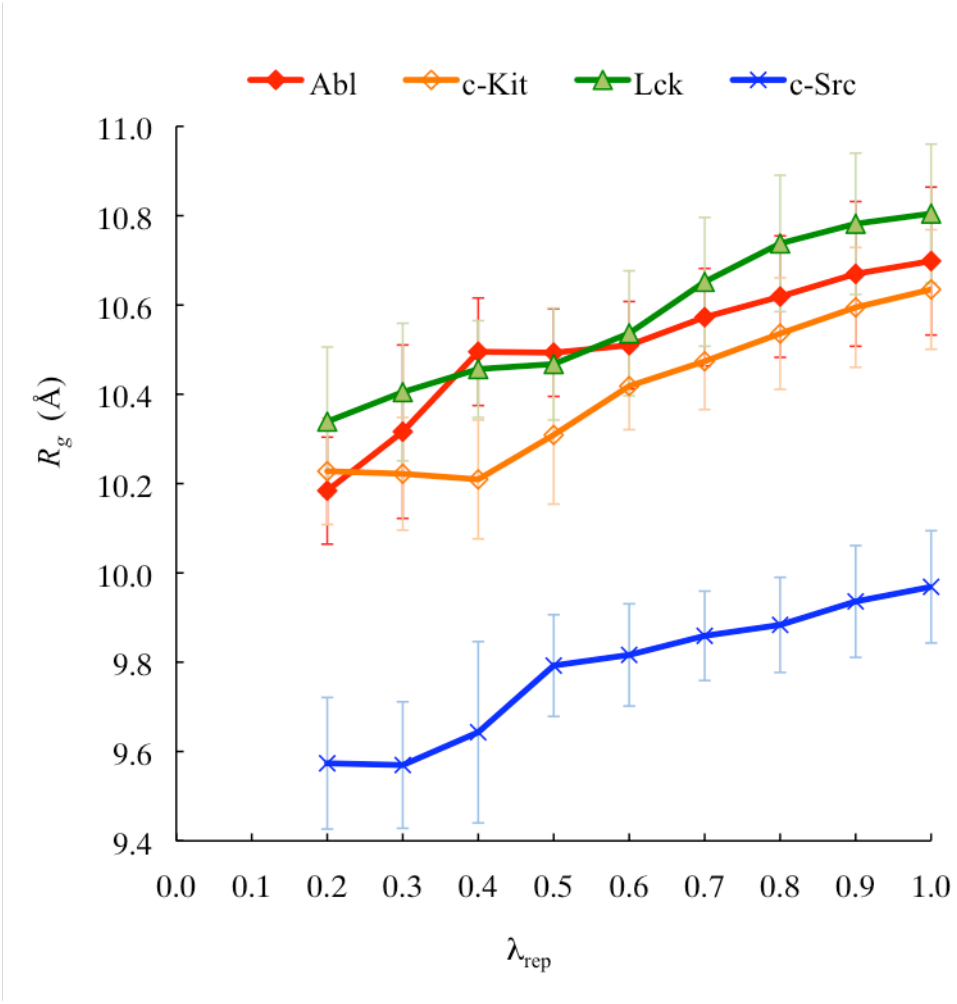

Figure S6: Radius of gyration, R_g, for the binding site residues of Abl, c-Kit, Lck, and c-Src as a function of the coupling parameter λ_{rep}, which is obtained by averaging over the last 1100 configurations saved during the FEP calculations. The standard deviation of the mean is shown. For each system, the apo structure was initially equilibrated for 2 ns, and 100 configurations saved from the last 200-ps equilibration simulation were used to obtain the average position of the center of mass of the residues in the binding pocket, i.e. $\langle R_C \rangle$. Each configuration used to compute R_g was first superimposed with respect to the last apo configuration saved from the equilibration before carrying out the radius of gyration calculations. Radius of gyration is defined as $R_g^2 = \sum m_i \left(r_i - \langle R_C \rangle\right)^2 / M$, in which r_i is the position, m_i is the mass of the selected atom, and M is the total mass of the selected atoms.

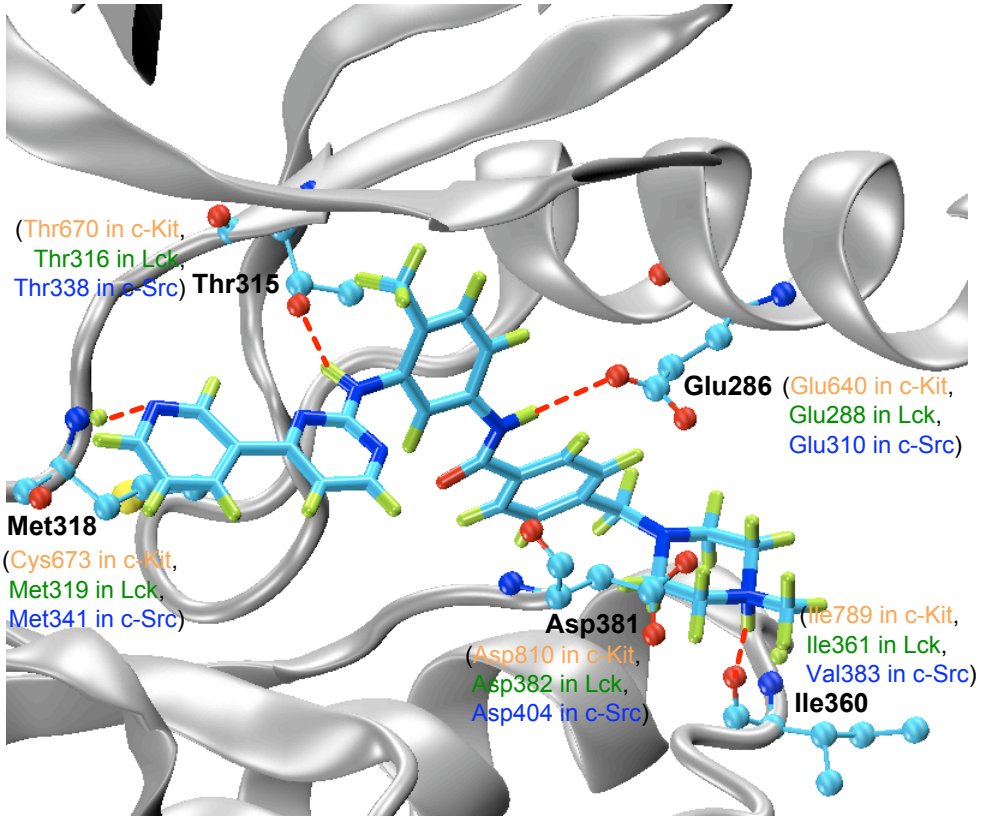

Figure S7: Snapshot of hydrogen-bonding network in the Gleevec-bound pocket of Abl kinase. Only certain key residues (discussed in text) and their hydrogen-bonding patterns are shown for the sake of clarify. The corresponding residues in c-Kit, Lck, and c-Src kinases are described in parentheses. The loop-sheet-motif of Abl is shown in silver. Gleevec is shown in thick sticks. The key residues are shown in ball-and-stick. Carbon, oxygen, nitrogen, sulfur and hydrogen atoms are colored cyan, red, blue, yellow, and lime, respectively.

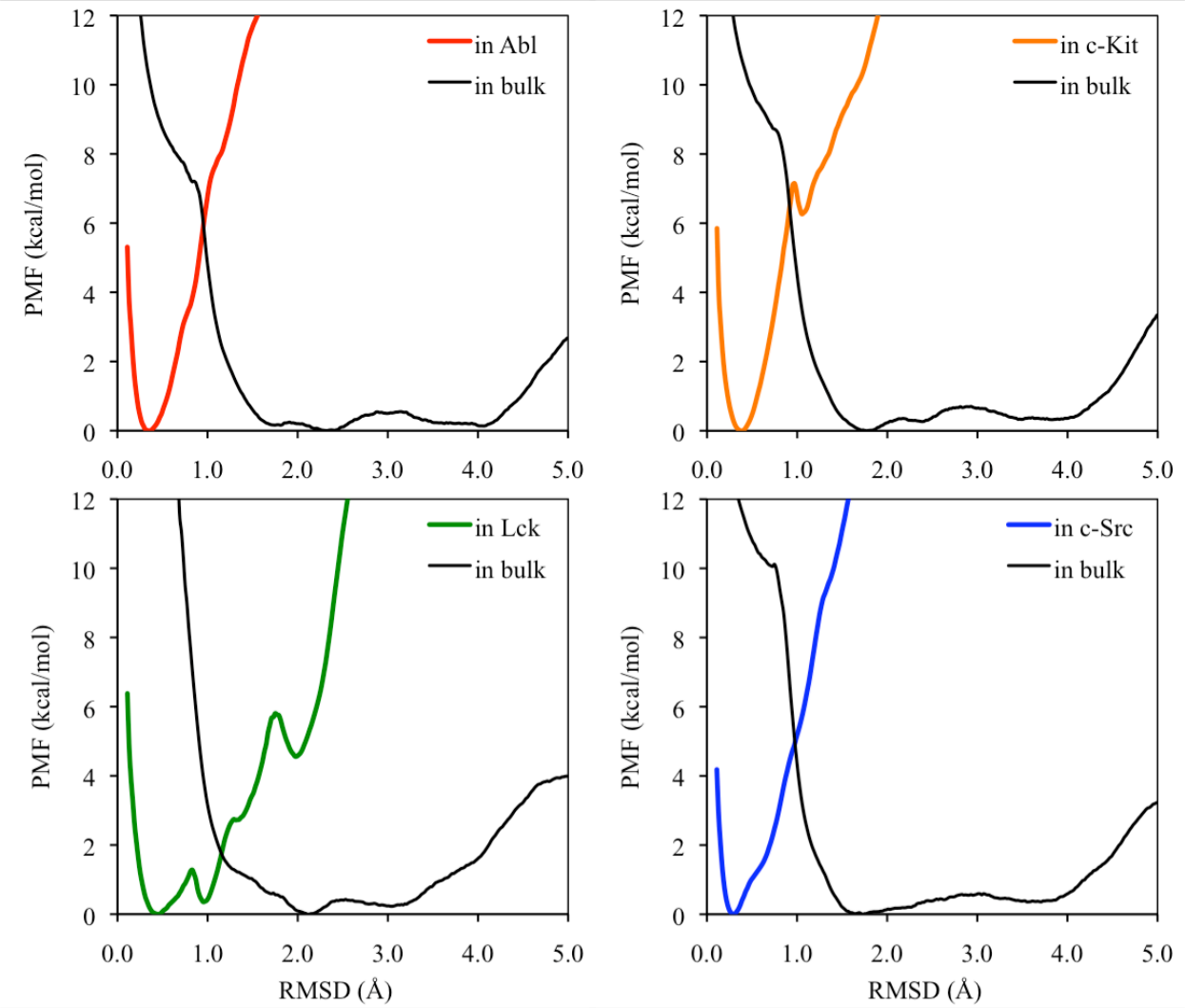

Figure S8: PMF profiles on the conformational restraints for Gleevec in bulk solution (black line) as well as in the binding pockets of Abl (red line), c-Kit (orange line), Lck (green line), and c-Src (blue line)

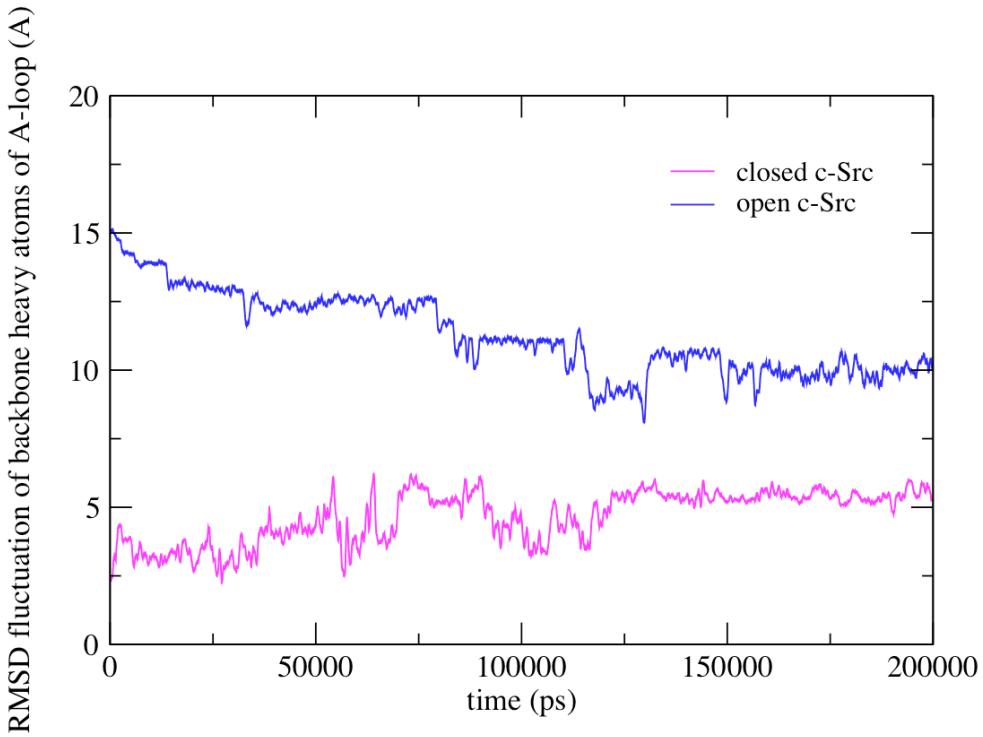

Figure S9: RMSD versus simulation time for the backbone heavy atoms of the closed-form (in magenta color) and open-form (in blue color) A-loop in c-Src structure complexed with Gleevec relative to the initial c-Src structure in which the A-loop is in closed-form conformation. For each protein-ligand complex systems, the overall structure and the position of the A-loop are stable in the course of the MD trajectories, indicating that the closed and open-form conformations of A-loop are two stable and representative states to be considered in the ligand-bound simulations.

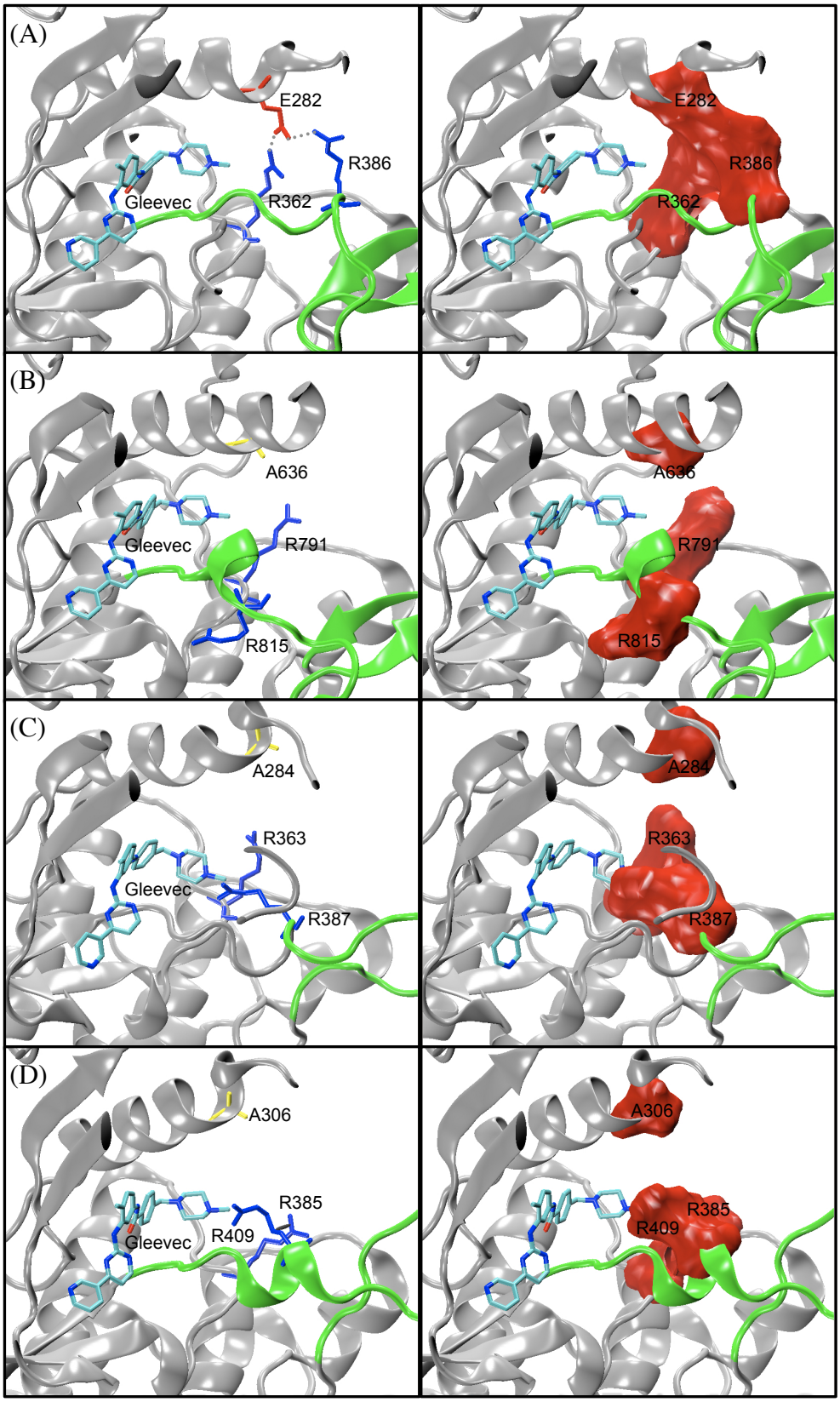

Figure S10: Ribbon diagram of (A) Abl, (B) c-Kit, (C) Lck, and (D) c-Src in complex with Gleevec. Gleevec is represented by sticks. *Left panel*: key hydrogen bonds are highlighted as dashed lines. *Right panel*: surface representation of the key residues

Table S1. Restraint on the ligand. P_{cm} and L_{cm} are the center of mass (COM) of the protein and ligand, respectively. P_1 and P_2 are the COM of the heavy atoms of selected protein residues. L_1 and L_2 are the COM of selected ligand atoms. These six point-positions were used to define the relative position and orientation of the ligand with respect to the target protein.

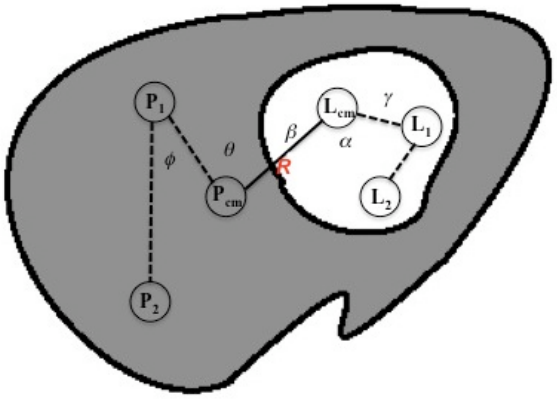

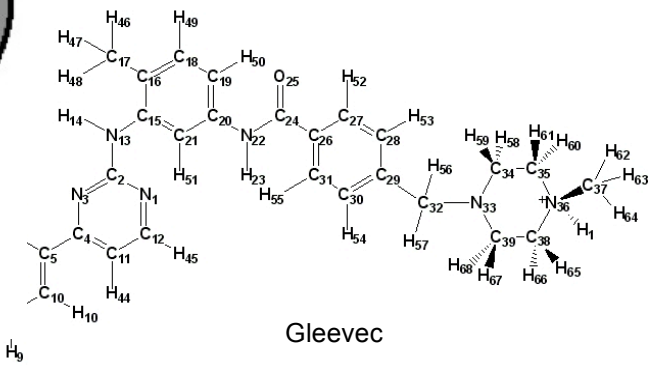

	Abl	c-Kit	Lck	c-Src(*c*)	c-Src(*o*)
P_1	Lys274	Val654	Glu310	His319	Arg179
P_2	Ser410	Lys913	Ala368	Leu360	Arg210
L_1	C_{23}, C_{25}, N_5	C_{37}, C_{38}, N_{36}	C_{34}, C_{35}, N_{36}	C_4, C_5, H_{45}	C_{27}, C_{28}, C_{29}
L_2	C_5, C_7, N_2	C_4, C_{11}, C_{12}	C_4, C_5, C_{11}	C_{26}, C_{27}, C_{28}	N_7, C_8, C_6
r	7.5	8.3	7.7	9.2	8.9
θ	121.6	135.2	103.8	65.2	121.7
ϕ	35.0	–49.0	–14.7	–147.8	–103.2
α	63.9	73.5	58.0	89.4	63.8
β	20.6	–23.7	131.1	105.2	98.7
γ	–61.1	–60.8	–40.8	–45.1	70.0

Unit: distance in Å; angle in degree

Table S2. Averaged dispersive (E_{dis}) contributions to the interactions energy between the protein residues and Gleevec in the binding pockets of Abl, c-Kit, Lck, and c-Src[a,b]

Abl		c-Kit		Lck		c-Src(*c*)		c-Src(*o*)	
residue	E_{dis}	residue	E_{dis}	residue	E_{dis}	residue	E_{dis}	residue	E_{dis}
L248	-2.27	L595	-2.99	L251	-2.33	L273	-2.05	L273	-2.42
G249	-0.11	G596	-0.24	G252	-0.14	G274	-0.07	G274	-0.17
G250	-0.02	A597	-0.04	A253	-0.05	Q275	-0.02	Q275	-0.08
G251	-0.03	G598	-0.01	G254	-0.04	G276	-0.02	G276	-0.04
Q252	-0.15	A599	0.00	Q255	-0.03	C277	0.00	C277	-0.01
Y253	-3.42	F600	0.00	F256	-0.03	F278	0.00	F278	-0.03
G254	-0.10	G601	-0.02	G257	-0.05	G279	-0.02	G279	-0.06
E255	-0.14	K602	-0.14	E258	-0.12	E280	-0.09	E280	-0.15
V256	-3.16	V603	-3.32	V259	-2.73	V281	-1.64	V281	-2.96
Y257	-0.33	V604	-0.30	W260	-0.33	W282	-0.29	W282	-0.38
A269	-2.39	A621	-2.56	A271	-2.46	A293	-2.67	A293	-2.50
V270	-1.08	V622	-1.22	V272	-1.23	I294	-1.22	I294	-1.23
K271	-2.28	K623	-2.83	K273	-2.76	K295	-2.65	K295	-2.85
V280	0.00	R634	0.00	P282	0.00	P304	0.00	P304	0.00
E281	0.00	E635	-0.0	D283	0.00	E305	0.00	E305	0.00
E282	-0.07	A636	-0.05	A284	0.01	A306	-0.04	A306	-0.08
F283	-0.16	L637	-0.21	F285	0.15	F307	-0.16	F307	-0.16
L284	-0.02	M638	-0.03	L286	-0.05	L308	-0.04	L308	-0.04
K285	-0.19	S639	-0.12	A287	-0.08	Q309	-0.14	Q309	-0.12
E286	-2.01	E640	-2.53	E288	-2.75	E310	-2.61	E310	-2.65
A287	-0.16	L641	-0.26	A289	-0.27	A311	-0.32	A311	-0.29
A288	-0.08	K642	-0.09	N290	-0.08	Q312	-0.11	Q312	-0.10
V289	-2.04	V643	-1.82	L291	-2.09	V313	-1.87	V313	-1.65
M290	-4.32	L644	-3.43	M292	-4.29	M314	-5.06	M314	-5.12
K291	-0.07	S645	-0.07	K293	-0.07	K315	-0.10	K315	-0.10
E292	-0.10	Y646	-0.10	Q294	-0.08	K316	-0.10	K316	-0.10
I293	-1.93	L647	-1.41	L295	-1.23	L317	-1.35	L317	-1.45
K294	-0.04	G648	-0.04	Q296	-0.05	R318	-0.05	R318	-0.07
L298	-1.24	I653	-1.14	L300	-1.13	L322	-1.38	L322	-1.35
V299	-2.82	V654	-2.61	V301	-1.94	V323	-2.00	V323	-2.23
I313	-2.04	V668	-1.60	I314	-1.96	I336	-1.62	I336	-1.89
I314	-0.58	I669	-0.61	I315	-0.65	V337	-0.56	V337	-0.71
T315	-2.68	T670	-2.67	T316	-2.91	T338	-2.97	T338	-2.95
E316	-0.86	E671	-0.84	E317	-0.47	E339	-0.94	E339	-0.81
F317	-2.87	Y672	-2.90	Y318	-2.60	Y340	-2.50	Y340	-2.83
M318	-2.84	C673	-2.30	M319	-1.81	M341	-2.35	M341	-2.31
T319	-0.33	C674	-0.32	E320	-0.30	S342	-0.23	S342	-0.26
Y320	-0.23	Y675	-0.18	N321	-0.20	K343	-0.15	K343	-0.19
G321	-0.84	G676	-0.78	G322	-0.99	G344	-0.82	G344	-0.92
N322	-0.32	D677	-0.30	S323	-0.42	S345	-0.34	S345	-0.36
L354	-1.67	L783	-1.42	I355	-0.26	V377	-0.69	V377	-0.52
F359	-2.38	C788	-1.65	Y360	-0.21	Y382	-2.17	Y382	-1.71
I360	-2.48	I789	-1.81	I361	-0.69	V383	-2.47	V383	-1.74

H361	-3.10	H790	-3.52	H362	-4.03	H384	-2.97	H384	-3.88
R362	-2.51	R791	-1.52	R363	-1.80	R385	-1.04	R385	-1.89
D363	-0.20	D792	-0.26	D364	-1.63	D386	-0.20	D386	-0.25
L370	-3.12	L799	-3.12	L371	-3.27	L393	-3.00	L393	-3.16
V379	-0.90	I808	-1.13	I380	-1.03	V402	-0.74	V402	-0.73
A380	-2.43	C809	-4.10	A381	-2.58	A403	-2.53	A403	-2.15
D381	-5.66	D810	-4.78	D382	-6.25	D404	-5.52	D404	-5.49
F382	-2.06	F811	-2.55	F383	-3.37	F405	-2.45	F405	-3.04
G383	-0.17	G812	-0.16	G384	-0.23	G406	-0.16	G406	-0.29
L384	-0.08	L813	-0.20	L385	-0.13	L407	-0.09	L407	-0.11
S385	-0.03	A814	-0.59	A386	-0.04	A408	-0.02	A408	-0.17
R386	-0.03	R815	-0.15	R387	-2.43	R409	-0.88	R409	-0.21
-		D816	0.00	-		-		-	
L387	-0.01	I817	0.00	L388	-0.02	L410	0.00	L410	-2.52
M388	0.00	K818	0.00	I389	0.00	I411	0.00	I411	-2.07
T389	0.00	N819	0.00	E390	0.00	E412	0.00	E412	-0.17
G390	0.00	D820	0.00	D391	0.00	D413	0.00	D413	-0.04
D391	0.00	S821	0.00	N392	0.00	N414	0.00	N414	-0.02
T392	0.00	N822	0.00	E393	0.00	E415	0.00	E415	0.00
Y393	-0.01	Y823	0.00	Y394	0.00	Y416	0.00	Y416	-0.05
T394	0.00	V824	0.00	T395	0.00	T417	0.00	T417	0.00
A395	0.00	V825	0.00	A396	0.00	A418	0.00	A418	0.00
H396	0.00	K826	0.00	R397	0.00	R419	0.00	R419	0.00
A397	0.00	G827	0.00	E398	0.00	Q420	0.00	Q420	0.00
G398	0.00	N828	0.00	G399	0.00	G421	0.00	G421	0.00
A399	0.00	A829	0.00	A400	0.00	A422	0.00	A422	0.00
K400	0.00	R830	0.00	K401	0.00	K423	0.00	K423	0.00
F401	0.00	L831	0.00	F402	-0.03	F424	0.00	F424	0.00
P402	0.00	P832	0.00	P403	0.00	P425	0.00	P425	0.00
site[c]	-71.12	site[c]	-67.03	site[c]	-66.88	site[c]	-63.45	site[c]	-71.74
water[d]	-0.74	water[d]	-1.97	water[d]	-1.54	water[d]	-1.67	water[d]	3.79
total	-71.86	total	-69.00	total	-68.42	total	-65.12	total	-67.95

[a] Unit in kcal/mol. [b] 1,100 configurations of the last 1.1 ns simulations were used. [c] By summing up the individual interaction energy of the binding site residue. [d] Water within 3.0 Å of the ligand of each configuration are considered.

Table S3. Averaged electrostatic (E_{elec}) contributions to the interactions energy between the protein residues and Gleevec in the binding pockets of Abl, c-Kit, Lck, and c-Src[a,b]

Abl		c-Kit		Lck		c-Src(*c*)		c-Src(*o*)	
residue	E_{elec} [a]	residue	E_{elec} [a]	residue	E_{elec} [a]	residue	E_{elec} [a]	residue	E_{elec} [a]
L248	-0.05	L595	-0.17	L251	-0.25	L273	0.21	L273	0.02
G249	0.01	G596	-0.01	G252	0.01	G274	0.00	G274	0.00
G250	0.00	A597	0.00	A253	-0.01	Q275	0.00	Q275	0.00
G251	0.00	G598	0.00	G254	0.00	G276	0.00	G276	0.00
Q252	0.00	A599	0.00	Q255	-0.01	C277	0.00	C277	0.00
Y253	0.08	F600	0.00	F256	0.00	F278	0.00	F278	0.00
G254	-0.01	G601	0.00	G257	0.00	G279	0.00	G279	0.00
E255	0.00	K602	0.00	E258	-0.01	E280	-0.01	E280	-0.01
V256	0.07	V603	-0.11	V259	-0.10	V281	-0.02	V281	-0.06
Y257	0.00	V604	0.00	W260	-0.01	W282	0.00	W282	0.00
A269	-0.26	A621	-0.34	A271	-0.09	A293	-0.27	A293	-0.17
V270	0.11	V622	0.14	V272	0.10	I294	0.10	I294	0.10
K271	0.69	K623	0.10	K273	0.36	K295	0.37	K295	0.17
V280	0.00	R634	0.00	P282	0.00	P304	0.00	P304	0.00
E281	0.00	E635	0.00	D283	0.00	E305	0.00	E305	0.00
E282	-0.01	A636	0.00	A284	0.00	A306	0.00	A306	0.00
F283	0.00	L637	0.02	F285	0.00	F307	-0.02	F307	0.00
L284	0.00	M638	0.00	L286	0.00	L308	0.00	L308	0.00
K285	0.01	S639	-0.01	A287	0.00	Q309	-0.01	Q309	0.00
E286	-5.24	E640	-4.32	E288	-5.65	E310	-3.76	E310	-5.10
A287	-0.01	L641	-0.02	A289	-0.01	A311	-0.02	A311	-0.01
A288	0.00	K642	0.00	N290	0.00	Q312	0.00	Q312	0.00
V289	0.43	V643	0.47	L291	0.39	V313	0.52	V313	0.31
M290	-0.14	L644	0.31	M292	-0.45	M314	-0.16	M314	-0.21
K291	0.00	S645	0.00	K293	0.00	K315	0.00	K315	0.00
E292	0.00	Y646	0.00	Q294	0.00	K316	0.00	K316	0.00
I293	0.16	L647	0.19	L295	0.12	L317	0.35	L317	0.25
K294	0.00	G648	0.00	Q296	0.00	R318	0.00	R318	0.00
L298	0.05	I653	0.02	L300	0.04	L322	0.07	L322	0.12
V299	-0.25	V654	-0.24	V301	-0.26	V323	-0.22	V323	-0.18
I313	-0.13	V668	-0.26	I314	-0.31	I336	-0.27	I336	-0.14
I314	0.06	I669	0.07	I315	0.08	V337	0.06	V337	0.05
T315	-4.29	T670	-4.16	T316	-2.20	T338	-3.87	T338	-3.21
E316	-0.45	E671	-0.51	E317	-0.34	E339	-0.45	E339	-0.50
F317	-1.73	Y672	-1.64	Y318	0.26	Y340	-1.84	Y340	-1.49
M318	-5.38	C673	-5.44	M319	-0.75	M341	-5.09	M341	-5.19
T319	-0.02	C674	0.00	E320	-0.08	S342	-0.02	S342	-0.01
Y320	0.02	Y675	0.01	N321	0.03	K343	0.01	K343	0.02
G321	0.46	G676	0.33	G322	-0.07	G344	0.42	G344	0.41
N322	0.05	D677	0.00	S323	-0.15	S345	0.04	S345	0.07
L354	0.32	L783	0.22	I355	0.05	V377	0.19	V377	0.04
F359	1.12	C788	1.11	Y360	0.06	Y382	1.35	Y382	0.11

I360	-9.17	I789	-9.67	I361	-1.64	V383	-8.64	V383	-1.69
H361	-4.72	H790	-3.04	H362	-10.41	H384	-4.19	H384	-11.07
R362	1.39	R791	1.26	R363	1.01	R385	0.36	R385	-0.02
D363	0.03	D792	0.03	D364	-6.28	D386	0.04	D386	-1.50
L370	0.07	L799	0.01	L371	-0.08	L393	0.10	L393	0.07
V379	0.10	I808	0.17	I380	0.05	V402	0.11	V402	0.00
A380	-1.03	C809	-1.42	A381	-1.08	A403	-1.21	A403	-1.29
D381	-5.70	D810	-4.80	D382	-4.85	D404	-2.90	D404	-5.92
F382	-0.10	F811	-0.24	F383	-0.17	F405	0.09	F405	-0.08
G383	0.04	G812	0.02	G384	0.02	G406	0.01	G406	0.12
L384	0.00	L813	0.00	L385	0.00	L407	0.00	L407	0.04
S385	0.00	A814	0.01	A386	0.01	A408	0.00	A408	0.47
R386	0.00	R815	0.02	R387	3.90	R409	1.44	R409	-0.04
-		D816	0.00	-		-		-	-0.26
L387	0.00	I817	0.00	L388	0.00	L410	0.00	L410	0.49
M388	0.00	K818	0.00	I389	0.00	I411	0.00	I411	0.04
T389	0.00	N819	0.00	E390	0.00	E412	0.00	E412	0.00
G390	0.00	D820	0.00	D391	0.00	D413	0.00	D413	0.00
D391	0.00	S821	0.00	N392	0.00	N414	0.00	N414	0.00
T392	0.00	N822	0.00	E393	0.00	E415	0.00	E415	0.00
Y393	0.00	Y823	0.00	Y394	0.00	Y416	0.00	Y416	0.00
T394	0.00	V824	0.00	T395	0.00	T417	0.00	T417	0.00
A395	0.00	V825	0.00	A396	0.00	A418	0.00	A418	0.00
H396	0.00	K826	0.00	R397	0.00	R419	0.00	R419	0.00
A397	0.00	G827	0.00	E398	0.00	Q420	0.00	Q420	0.00
G398	0.00	N828	0.00	G399	0.00	G421	0.00	G421	0.00
A399	0.00	A829	0.00	A400	0.00	A422	0.00	A422	0.00
K400	0.00	R830	0.00	K401	0.00	K423	0.00	K423	0.00
F401	0.00	L831	0.00	F402	0.01	F424	0.00	F424	0.00
P402	0.00	P832	0.00	P403	0.00	P425	0.00	P425	0.02
site[c]	-33.43	site[c]	-31.90	site[c]	-28.77	site[c]	-27.08	site[c]	-35.29
water[d]	-22.73	water[d]	-29.82	water[d]	-36.33	water[d]	-26.29	water[d]	-19.94
total	-56.16	total	-61.72	total	-65.10	total	-53.37	total	-55.23

[a] Unit in kcal/mol. [b] 1,100 configurations of the last 1.1 ns simulations were used. [c] By summing up the individual interaction energy of the binding site residue. [d] Water within 3.0 Å of the ligand of each configuration are considered.